GEOPHYSICS, VOL. 80, NO. 3 (MAY-JUNE 2015); P. WB11–WB19, 5 FIGS., 3 TABLES.
10.1190/GEO2014-0119.1

Soil density, elasticity, and the soil-water characteristic curve inverted from field-based seismic P- and S-wave velocity in shallow nearly saturated layered soils

Jie Shen[1], Juan M. Lorenzo[1], Chris D. White[2], and Frank Tsai[3]

ABSTRACT

Soil density, porosity, elastic moduli, and the soil-water characteristic curve (SWCC) are important properties for soil characterization. However, geotechnical and laboratory tests for soil properties are costly and limited to point sampling sites. Seismic surveys can provide laterally continuous, seismic soil property values that may complement geotechnical borehole tests with less cost. We have developed a workflow to invert for soil properties and the SWCC from seismic P- and S-wave velocity-versus-depth profiles interpreted from shallow (<25 m depth) unconsolidated sediments under conditions of near-full saturation (>99%). The inversion is performed by using the covariance matrix adaptation evolution strategy to search automatically for optimal input soil property values by minimizing the misfit between field-based velocity profiles and predicted velocity profiles based on the Hertz-Mindlin and Biot-Gassmann theories. The results from seismic soil property inversion are validated by comparison with geotechnical as well as laboratory results conducted independently in the same area as the seismic survey. For each seismically recognizable layer, soil types are interpreted from the inverted soil density and elasticity, aided by the SWCC to help detect thin units that are below the original seismic resolution of the field data. There is flexibility to apply our suggested workflow in future studies. For a known geologic setting, empirical relationships and other velocity prediction models could also be incorporated into the suggested workflow to improve inversion results and extract additional information in soils.

INTRODUCTION

Soil properties such as density, elastic moduli, porosity, and the soil-water characteristic curve (SWCC) are important for assessing foundation stability (Bell, 1992), and monitoring contaminant movement and soil aeration (Terzaghi, 1996). These soil properties depend on soil grain size, mineral composition, overburden pressure, and stress history (Fredlund and Xing, 1994). Soil properties can be measured directly in the laboratory (Van Genuchten, 1980), but these tests are costly, and the necessary equipment may not be readily accessible. Laboratory soil property tests are performed on either core or bulk sediment samples, which may not be representative of in situ sediments. The borehole locations are usually distant from each other (>100's of meters), so that lateral soil characteristics between boreholes are difficult to predict.

In this paper, we use an indirect inversion process to determine in situ soil density, elastic moduli, porosity, and the SWCC by minimizing the misfit (cost function) between the predicted and field-derived velocity profiles (Figure 1). To perform the inversion, an optimization technique automatically searches for input soil-property-parameter values that can best explain the field velocity profiles. Compared with other seismic inversion techniques (such as the widely used full-waveform inversion), the major advantages of our inversion are that it uses a global optimization technique and requires only a velocity-versus-depth profile, which is interpreted from the seismic survey. A global optimization technique searches for a global minimal value of the misfit throughout the input parameter range. Unlike local optimization, which is used by full-waveform inversion, global optimization is not affected

Manuscript received by the Editor 9 March 2014; revised manuscript received 6 September 2014; published online 23 April 2015.
[1]Louisiana State University, Department of Geology and Geophysics, Baton Rouge, Louisiana, USA. E-mail: jshen6@lsu.edu; gllore@lsu.edu.
[2]Louisiana State University, Craft and Hawkins Department of Petroleum Engineering, Baton Rouge, Louisiana, USA. E-mail: cdwhite@lsu.edu.
[3]Louisiana State University, Department of Civil and Environmental Engineering, Baton Rouge, Louisiana, USA. E-mail: ftsai@lsu.edu.

by starting parameters. Currently, full-waveform inversion often relies on reflections (Masoni et al., 2014), which can be hard to get in shallow near-saturated soils because of attenuation, especially for P-waves. For our inversion, we incorporate refraction and reflection first arrivals through 1D P- and S-wave velocity-versus-depth starting models (Lorenzo et al., 2014). Moreover, the inversion of 1D velocity models is simpler and faster computationally than 2D or 3D waveform matching.

The SWCC shows the relationship between water saturation and the capillary head (Van Genuchten, 1980), both of which are readily determined in our inversion. At the same capillary head, water saturation increases with soil plasticity (Fredlund and Xing, 1994). Therefore, water saturation is lower in sandy soils than in clayey soils. The SWCC is used to estimate other soil behavior parameters such as unsaturated shear strength, permeability, and pore-size distribution (Fredlund and Rahardjo, 1993a; Fredlund, 1995; Fredlund et al., 1996).

Our velocity prediction model is based on the Hertz-Mindlin contact theory (Hertz, 1882; Mindlin, 1949) and the Biot-Gassmann fluid substitution theory (Gassmann, 1951; Biot, 1962) because they are the currently acceptable constitutive models used to relate effective elasticity and soil properties in shallow unconsolidated sediments (Bachrach et al., 1998; Bachrach and Nur, 1998; Bachrach et al., 2000; Zimmer et al., 2006; Bachrach and Avseth, 2008; Dutta et al., 2010). The Hertz-Mindlin model uses grain elasticity, porosity, and grain contact geometry under effective stress (Digby, 1981; Walton, 1987; Dvorkin and Nur, 1996) to calculate the isotropic elastic moduli of a homogeneous, granular matrix comprising identical spherical grains. The Hertz-Mindlin model also assumes dry, no-slip, spherical contacts between the grains, and as a result, Poisson's ratio for the grains is expected to be <0.25. The Biot-Gassmann fluid substitution theory accounts for pore fluid variation in a porous medium and estimates effective elastic moduli from dry matrix elasticity, grain elasticity, and water saturation. The Biot-Gassmann theory more accurately predicts velocities for data at low frequencies (10–200 Hz) than at higher frequencies (>10 kHz) in unconsolidated soil (Wang, 2001). Seismic velocity is ultimately computed from the relationships between velocity, effective elasticity, and bulk density (e.g., Ikelle and Amundsen, 2005).

The application of the Hertz-Mindlin model in clay-dominant sediments is debatable because the model is originally derived using spherical grains. For example, shear modulus is overestimated by Hertz-Mindlin for angular grains (Bachrach et al., 2000) and clay grains have a platy shape. One heuristic approach is to lower the coordination number for computing predicted velocities of angular grains (Bachrach et al., 1998; Velea et al., 2000). Particularly in shallow unconsolidated sediments, loosely packed, highly angular grains lead to a lower coordination number and higher porosity. As a result, high-porosity (~65%) clay has a relatively lower coordination number than medium-porosity (~40%) sand (Murphy, 1982). The Hertz-Mindlin theory predicts elastic moduli successfully in clay-dominant rocks, such as shales (Avseth et al., 2005) and claystones (Takahashi and Tanaka, 2009).

Additional debate surrounds the application of a high Poisson's ratio (>0.25) with the Hertz-Mindlin theory in wet sediments. In saturated unconsolidated sands (e.g., Dvorkin and Nur, 1996), as well as in almost fully saturated clays (such as in our case), the effective Poisson's ratio can be larger than 0.25. Dvorkin and Nur (1996) use the Hertz-Mindlin theory to predict velocities successfully in saturated loose sands with a high effective Poisson's ratio close to 0.5.

Another factor that needs to be considered for clay at shallow depth when using the Hertz-Mindlin model is the effective stress. In sand, the dominant stresses are overburden pressure and matric suction (cohesion is close to 0), whereas in clay, cohesion (up to 20 kPa) also plays a significant role. In this study, we modify the effective stress by also incorporating the effect of matric suction and cohesion. This modification helps to predict velocities in agreement with field velocities in clay-and-sand mixed soils (Crane, 2013).

Among the various optimization algorithms used to effectively search for those parameters that explain field velocity profiles, we use the covariance matrix adaptation evolution strategy (CMA-ES) (Hansen, 2011). CMA-ES belongs to the class of evolutionary algorithms, and it is a stochastic, derivative-free algorithm used for nonlinear local and global optimization (Mezura-Montes and Coello Coello, 2011). One of the advantages in CMA-ES over the genetic algorithm is its well-designed, internal, parameter-tuning mechanism that selects new candidates for input parameter values while approaching a best fit between prediction and observation. The parameter-tuning mechanism is based on updating the covariance matrix between variables in the distribution (Hansen, 2011) as the candidate values converge toward the global optimum. In CMA-ES, population size is crucial to the success of global optimization — this number, by increasing logarithmically with the number of unknown inputs, is designed to avoid a local optimum (Hansen, 2006). CMA-ES is applied to model fluid flow (Bayer et al., 2009) and to facilitate groundwater remediation (Bayer and Finkel, 2007).

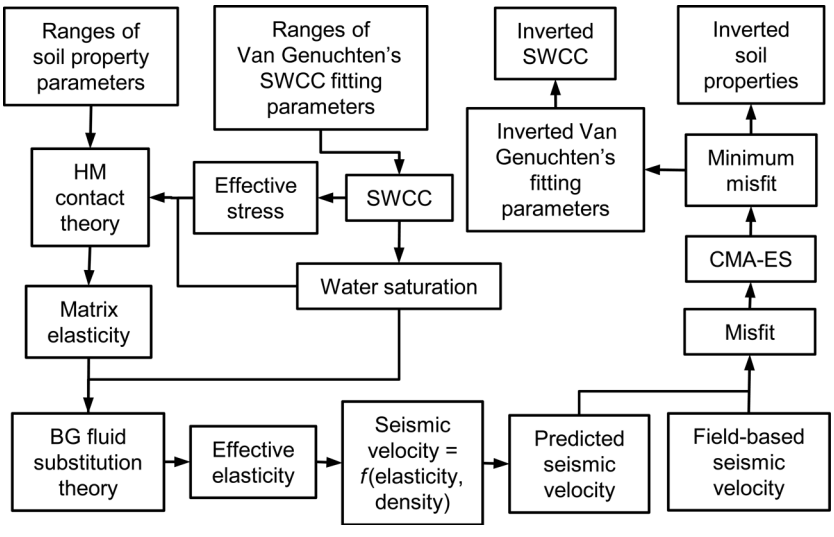

Figure 1. The procedure of soil property inversion by minimizing the misfit between predicted and field-based seismic velocities. Predicted velocities are calculated by the Hertz-Mindlin and Biot-Gassmann models. Covariance matrix adaptation evolution strategy (CMA-ES) is the optimization program to minimize misfit.

We attempt our inversion for seismic soil properties in almost fully saturated soils of the lower Mississippi River swamps and marshes (Lorenzo et al., 2014) because the seismic velocity is most sensitive to water saturation at near-saturation conditions (water saturation >99%). Near-saturated soils occur permanently or seasonally in wetlands, including coastal, floodplains, the margins of lakes, and other areas below groundwater level or where precipitation is sufficiently high (Gilman, 1994). The velocity prediction models (e.g., Bachrach and Nur, 1998) and field-based velocity profiles (e.g., Grelle and Guadagno, 2009) show that P-wave velocities change from ~200 to ~1500 m/s in the transition zone from near-saturated soils to saturated soils. As the soil approaches full saturation, the pore water substitutes almost all of the air. The bulk modulus of water is more than four orders of magnitude larger than that of air (Table 1). As a result, higher water saturation yields a stiffer soil with an increased compressional velocity. Because S-waves are insensitive to pore fluids and travel more slowly than P-waves, S-waves are less attenuated by fluids and have more resolution (Harris, 2009). As a result, S-waves are sensitive to soil type changes (Hayashi et al., 2013) and S-wave reflections can be used to identify soil layers.

METHODS

Field-based data

The field data we use for inversion include field-based P- and S-wave velocity-versus-depth profiles interpreted from seismic surveys at two field sites (Figure 2). The seismic survey is conducted in the almost fully saturated shallow soil (<25 m) beneath a New Orleans flood-protection levee (Lorenzo et al., 2014). In these data, the seismic frequency reaches 30 Hz. In velocity-versus-depth profiles, there is ±1 m error in layer depths (Lorenzo et al., 2014) and ±2% error in P- and S-wave velocities. The seismic survey line is ~100 m wide. As a result, the velocity profiles represent the average of the survey width. Two sites (A and B) help validate the inversion results under a variety of water-saturation conditions and sand and clay percentages. At both sites, the soil is composed of a majority of clay with several small sand units between the depths of 7.5 and 15 m, and these sand units are thicker at site A than at site B (Lorenzo et al., 2014).

Velocity prediction model

The Hertz-Mindlin contact theory and Biot-Gassmann fluid substitution theory (Appendix A) predict seismic velocities from soil properties, water saturation, and effective stress (Figure 1). Water saturation and effective stress are major factors that contribute to the increase in P-wave velocity from ~200 m/s to ~1200 m/s. In unconsolidated sediments, the Hertz-Mindlin model accounts for mechanical compaction from confining pressure, so that the predicted velocity is much more strongly dependent on effective stress than porosity (Avseth et al., 1998). In almost fully saturated soil (>99%), the velocity model predicts that a 1% change in water saturation leads to a 20% change in P-wave velocity, whereas a 1% change in soil properties (e.g., porosity, coordination number, density, and elasticity) leads to less than a 1% change in P-wave velocity. To explain field velocity increases with depth (Figure 2), we also need to relate the changes in water saturation and effective stress with depth. We use SWCC to predict the relationship between depth

Table 1. Key parameters with known values used in the Hertz-Mindlin and Biot-Gassmann models (Appendix A).

Parameters	Values
Water table (m)	36 (assumed for calculation)
g (m/s^2)	9.80665
ρ_w (kg/m^3)	1
ρ_a (kg/m^3)	1.18×10^{-3}
K_w (Pa)	2.2×10^9
K_a (Pa)	1.01×10^5

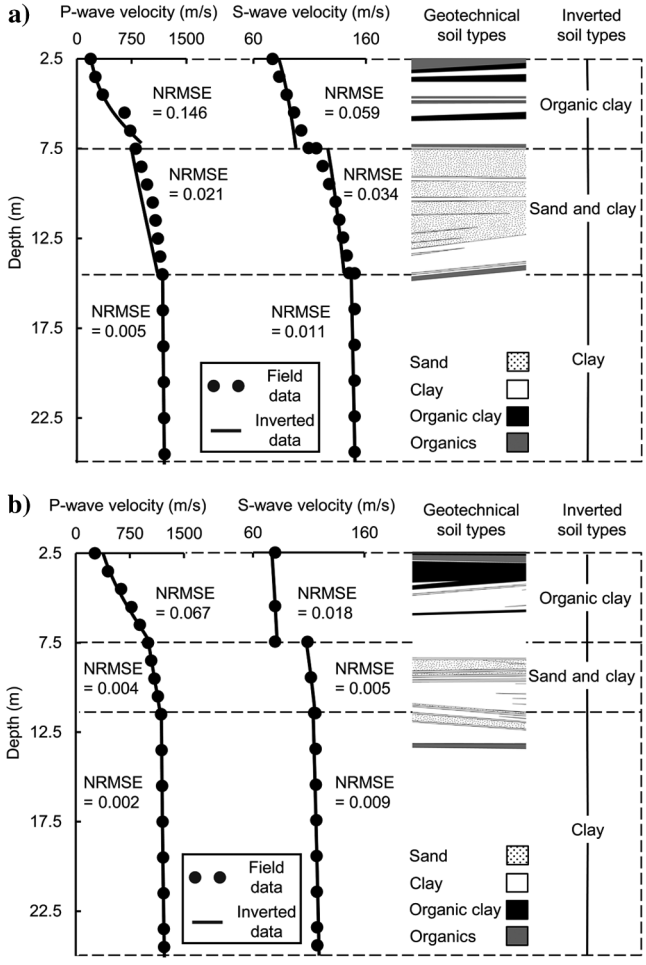

Figure 2. Predicted and field-based P- and S-wave velocity-versus-depth profiles and geotechnical cone penetration testing (CPT) soil type profiles from the seismic survey area (Lorenzo et al., 2014) at (a) site A and (b) site B. The quality of the inversion results can be quantified by the misfit between the field and predicted velocity-versus-depth profiles. Misfits are calculated by the sum of the normalized root-mean-square error (NRMSE) between the predicted and field velocity profiles. The CPT soil type profile shown here is 100 m wide and covers the same area as the seismic survey. At both sites, predicted velocities are calculated at discrete depths every 0.005 m. The depth error in the field velocity is ±1 m. The errors in field velocities are <2%. The soil types determined from the combination of density, elastic moduli, and SWCC are labeled for each layer.

and water saturation (Appendix A). Effective stress relates to the confining pressure as well as matric suction, and both of the parameters vary with depth. Density and elasticity (both matrix and effective) are calculated using water saturation and effective stress, which are themselves depth dependent (Figure 1).

Accurate prediction of seismic velocity in shallow (<25 m depth) unconsolidated sediments requires the incorporation of matric suction and cohesion into the estimation of effective stress in the Hertz-Mindlin and Biot-Gassmann models (Lu and Sabatier, 2009; Crane, 2013; Revil and Mahardika, 2013). In shallow, unconsolidated, clay-rich soil, matric suction and cohesion can be several orders of magnitude larger than overburden pressure and dominate effective stress (Lu and Sabatier, 2009). Rock physics models (Bachrach and Nur, 1998) indicate that seismic velocity is proportional to one-sixth of the power of the effective stress. The incorporation of matric suction and cohesion in clay-rich soil almost doubles the predicted seismic velocity and brings the results closer to real data (Crane, 2013). Cohesion is one kind of interparticle stress, and it arises from physicochemical forces between mineral grains. The matric suction is equal to the total stress difference at the air-water interface ($u_a - u_w$). In equilibrium, matric suction ($u_a - u_w$) around a capillary tube is balanced by the weight of the water column pulled up by surface tension (Fredlund and Rahardjo, 1993b):

$$(u_a - u_w) = \rho_w g h_c, \tag{1}$$

where u_a is the atmospheric pressure, u_w is the pore water pressure, h_c is the capillary head, ρ_w is the water density, and g is the gravitational acceleration (Table 1).

In shallow unconsolidated sediments, effective stress (P_{eff}) is the sum of the net overburden pressure ($\sigma - u_a$), matric suction ($u_a - u_w$), and cohesion (σ_{co}) (Lu and Likos, 2006):

$$P_{\text{eff}} = \sigma - u_a - S_w(u_a - u_w) + \sigma_{co}, \tag{2}$$

where σ is the overburden pressure and equals $\rho_{\text{eff}} g h$ (ρ_{eff} is the effective density of soil with pore fluids, and h is the depth of soil), u_a is the atmospheric pressure and is assumed to be zero, and $S_w(u_a - u_w)$ is the matric suction contribution weighted by the percentage of water saturation S_w (Lu and Sabatier, 2009).

Parameter constraint before inversion

CMA-ES optimization is accelerated by constraining the uncertainty of input parameter values within reasonable ranges (Table 2) for local soil types. Because our seismic survey was conducted on alluvial-deltaic soils (Lorenzo et al., 2014), the main soil types to consider are organic clay, clay, and sand. Organic clay has lower cohesion (Waltham, 2001) and larger compressibility than clay (Robertson, 1990) because of the organic residue in clay. Input parameters in the velocity prediction model include pore fluid properties, soil properties, and water-saturation related parameters. To give more flexibility to the search for optimal values by CMA-ES, we choose the largest published range of input parameter values for unconsolidated sediments (Table 2). For the correction of the overestimated shear modulus in the Hertz-Mindlin model, we use a coordination number of one, which is below a value with physical meaning. A coordination number of one is found to estimate velocity accurately in clay and sand mixtures (Crane, 2013). Pore fluids are assumed to be water and air, so their density and elastic properties are well known (Table 1). Because the maximum P-wave velocity throughout the profile is about 1400 m/s (Lorenzo et al., 2014) but below fully saturated velocity values, around 1500 m/s (Grelle and Guadagno, 2009), for the purpose of SWCC calculation, the water table (value of 36 m) is assumed to be slightly below the depth of the profile.

Table 2. The 11 unknown parameters with published ranges used in the Hertz-Mindlin and Biot-Gassmann models (Appendix A). The ranges of each parameter span those in organic clay, clay, and sand. These parameters are assumed to be constant within each seismically recognizable layer.

Parameters	Lower boundary	Upper boundary	References
ρ_0 (kg/m^3)	1.4	2.65	Walmsley (1977), Mavko et al. (2009)
K_0 (Pa)	3.4×10^6	3.66×10^{10}	Mittal et al. (2004), Mavko et al. (2009)
G_0 (Pa)	1.56×10^5	4.5×10^{10}	Mittal et al. (2004), Mavko et al. (2009)
ϕ	0.35	0.8	Nimmo (2004)
C	1	8	Crane (2013), Allen (1985)
σ_{co} (Pa)	0	2×10^4	Fredlund (1991), Bishop et al. (1960)
θ_r	0	0.436	Leong and Rahardjo (1997)
m	0	1	Van Genuchten (1980)
a	0	1	Van Genuchten (1980)
n	0	49.9	Van Genuchten (1980), Leong and Rahardjo (1997)

Table 3. Common soil density and dynamic elastic moduli values for three different soil types (organic clay, clay, and sand) used to calculate the average soil properties for each layer in a geotechnical soil model.

Soil type	Density (kg/m^3)	Bulk modulus (Pa)	Shear modulus (Pa)	References
Organic clay	1.4	3.4×10^6	1.56×10^5	Walmsley (1977), Mittal et al. (2004)
Clay	2.6	2.1×10^{10}	7×10^9	Mavko et al. (2009)
Sand	2.65	3.66×10^{10}	4.5×10^{10}	Mavko et al. (2009)

Seismic soil property inversion

Soil property inversion is carried out separately within each seismically recognizable layer. Soil properties and the three fitting parameters in SWCC (Table 2) are the outputs from inversion when the misfit between the predicted and field velocity profiles reaches its minimum. From the fitting parameters, we then compute inverted SWCCs with an assumed water table (value of

36 m) (Figure 1). Three seismic layers can be determined from sharp changes in the field-derived S-wave seismic velocity profiles for both sites (Figure 2). We use CMA-ES optimization to minimize the misfit between the field-velocity profile and the predicted velocity profile by varying the input soil-property parameter values within reasonable ranges (Table 2). The soil property parameters used to explain the field velocity profile are the optimal values that represent the local soil characteristics. Based on the assumptions of the velocity prediction model and considering the resolution of the seismic data, we assume that the sediments are homogeneous and isotropic within each seismic layer. As a result, soil properties (Table 2) are constant within each seismic layer. Soil properties represent average values over the width of seismic survey area (~100 m) and over the depth of each layer. At each depth, water saturation is an average of patchy saturation over the seismic survey area (~100 m). Our seismic data have effectively low frequency (≤30 Hz), so that pore fluid heterogeneity is unresolvable with the dominant seismic wavelet (Johnson, 2001). In each seismic layer, the misfit between the field velocity profile and the predicted velocity profile is quantified by the normalized root-mean-square error (NRMSE) at discrete depths every 0.005 m. NRMSE is calculated by normalizing the root-mean square of the difference between the predicted and field-based velocities by the average of the field-based velocities.

The ±2% velocity error and ±1-m depth error from the original field velocity data propagate into errors in the inverted soil properties and water saturation. For example, the depth error in the inverted results is ±1 m, which carries over from the depth errors (±1 m) in the field-based velocity model. We estimate the final inversion errors via a Monte Carlo simulation. First, we randomly generate 100 field-velocity-profile cases within their velocity error range of ±2%. Then, we invert for soil properties with the 100 different scenarios. The range of each resultant soil property value provides the estimated error.

Determination of soil types from inverted results

Inverted soil properties can be used to determine the soil types for each seismic layer by reference to published soil properties (Table 3). For different soil types, published density and elastic moduli vary over 70% (Table 3). Within single soil types, the variation in elastic moduli is about 20%–30% for clay, less than 5% for sand (Mavko et al., 2009), and about 50% for different organic clay (Mittal et al., 2004) because of different mineral content, overburden pressures, and organic content. We assign soil types based on where the inverted soil properties fall within these ranges. If the inverted soil property value lies outside the range for one soil type alone but between the values for two soil types, we consider that the soil type is a mixture of the two. Inverted soil property values that span the ranges of two or more soil types may indicate additional layering beyond the resolution of the seismic technique. SWCC can either be used to confirm a heterogeneity or locate thin units in a heterogeneous layer that may not be sensed by inverted density and elastic moduli values.

RESULTS

The predicted velocity-versus-depth profile matches the field velocity-versus-depth profile (Figure 2) in each of the three seismically recognizable layers with NRMSEs of less than 0.15 in all cases. The inverted density and elastic moduli correlate well in general with computed geotechnical results (Figure 3), except for the middle layer at site B (Figure 3b).

The inverted soil density, elastic moduli profiles, and the SWCC detect meaningful variations among three seismically recognizable layers and between sites A and B (Figures 3 and 4) as expected. The inverted soil property values are much larger at site A than at site B because the soil is sandier at the depth of the middle seismic layer (Figures 2 and 3).

The inverted water saturation, bulk density, and porosity values at site B are also in agreement within an error of 15% with independent laboratory results from a well near site B (Figure 5). The largest mismatch arises in the bulk density and porosity profiles in the first layer.

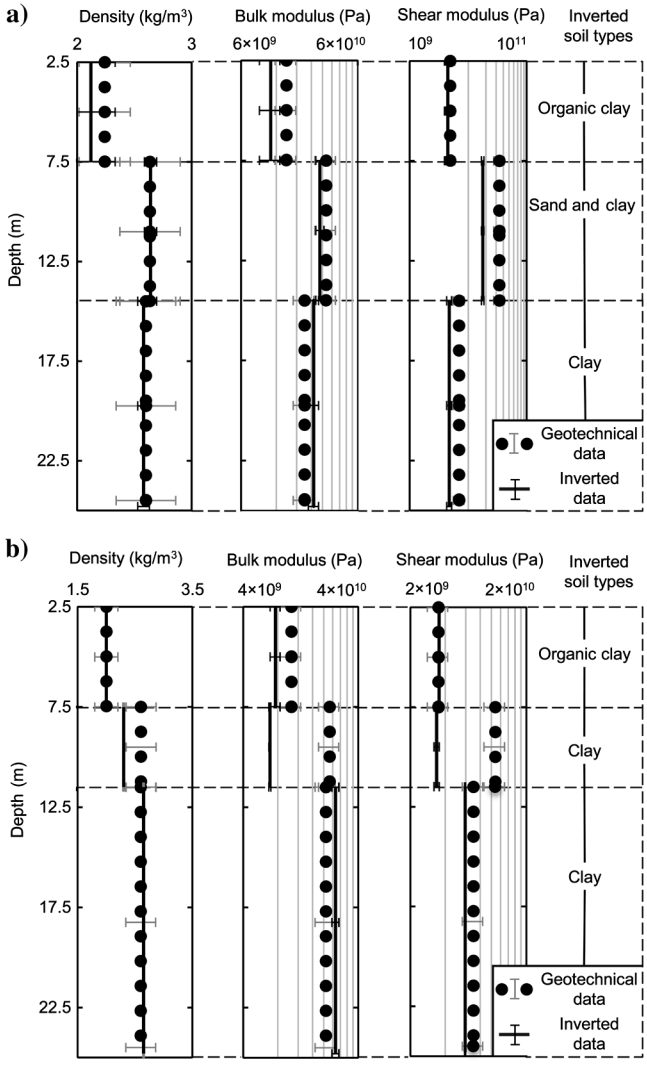

Figure 3. Density, bulk modulus, and shear modulus determined from seismic inversion and from geotechnical soil profile at (a) site A and (b) site B. The quality of the inverted soil properties can be quantified by the misfit between the inverted soil properties and the soil properties based on the CPT soil profile. For most layers, the inverted soil property values fall within the error ranges of geotechnical results. The largest misfit of 70% arises in the middle layer at site B. Soil types determined from inverted density and elastic moduli are labeled for each layer.

At sites A and B, the inverted soil properties show some common trends that can be used to identify the soil types within the three different seismic layers. In the top and bottom seismic layers, inverted soil density and elastic moduli values fall within the range for clay properties (Figure 3), but in addition, the relatively smaller values of the top seismic layer may indicate the presence of organic material. We note that for both sites, the water saturation (based on inverted SWCCs) shifts sharply to lower values across the top and bottom boundaries of the middle seismic layers (Figure 4). Laboratory data confirm a similar change to lower water saturation values at similar depths. For site A, the inverted soil density and elastic moduli values are relatively larger in the middle seismic layer than in the bottom layer. We interpret this to indicate that there may be additional sand within this clayey unit (Figure 3a, middle layer).

Soil types indicated by the inverted cohesion values are in agreement with soil types determined from the inverted density and elasticity. Inverted cohesion values in the bottom seismic layers at both sites are close to 20 kPa and indicate that the soil type is possibly clay. Inverted cohesion values in the top seismic layers are about 50% lower than in the bottom layers and may indicate the presence of less cohesive organics. In the middle seismic layer at site A, the inverted cohesion value is close to zero and indicates that the layer consists mainly of sand. In the middle seismic layer at site B, the inverted cohesion value is close to 20 kPa and indicates clayey soils.

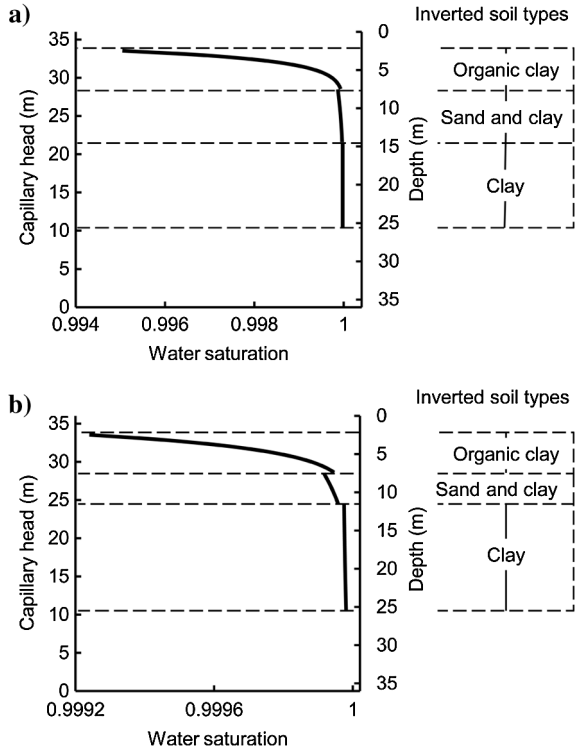

Figure 4. SWCCs from seismic inversion at (a) site A and (b) site B. The error in inverted SWCC is 0.1%. SWCC can help identify the heterogeneity within a layer. The shift of SWCC to a lower value within the middle layer indicates the presence of sand within the middle clay-dominant layer at both sites. Soil types determined from the combination of density, elastic moduli, and SWCC are labeled for each layer.

DISCUSSION

Validation of inversion results and interpretations

One measure of the usefulness of the inversion results for our three seismic layers is to compare them with other independent estimates of density and elastic moduli. If large differences appear between the two results, it may imply seismically unresolvable thin units. We assign known values of density and elasticity in soil (Table 3) to geotechnical soil-behavior types determined by cone penetration testing (CPT) (Lorenzo et al., 2014) (Figure 2) to calculate an average geotechnical density and elasticity for three new equivalent layers. The vertical resolution of the CPT soil profile is ±0.1 m. Computed geotechnical soil properties will have a range of values attributable to the variation of published soil properties (Table 3). A comparison of the inverted and computed geotechnical results of soil density and elastic moduli shows similar values and implications for soil types (Figure 3). The greatest difference between the inverted and geotechnical results occurs at depths equivalent to the middle layer at site B (Figure 3b), where the inverted elastic moduli are almost 70% lower than those from the CPT. One explanation for this big difference is the presence of thin sand units (<1 m) shown in the CPT soil profile (Figure 2b, the middle layer). When seismic waves pass through these thin units (<1 m at site B), the changes in soil density and elastic moduli may not be seismically resolvable. For example, a P-wave velocity of ~200–1200 m/s and a dominant frequency of 30 Hz suggest a dominant wavelength of ~7–40 m. These thin sand units lead to a larger computed geotechnical soil property values than the inverted results derived from seismic profiles. At site A, the sand layers are sufficiently thick. Thus, the inverted soil property values are closer to the geotechnical results and inverted soil types are comparable (Figures 2 and 3). These lateral differences in sand layer

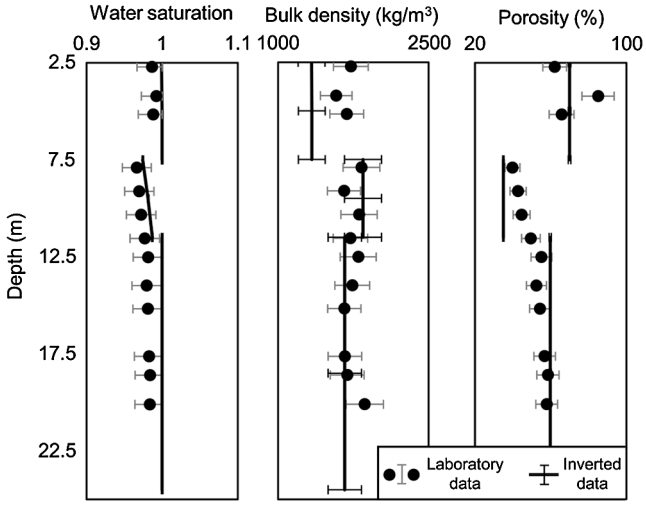

Figure 5. Water saturation, bulk density, and porosity from seismic inversion at site B and laboratory tests from a well near site B. The quality of the inversion can be quantified by differences between inverted and laboratory results. Inverted water saturations are within 2% of laboratory results. In the second and third layers, the inverted bulk density and the density are within 5% of laboratory results. In the first layer, the inverted bulk density and density differ by 15% from the laboratory results.

thickness may also be responsible for the noticeable differences in density and elastic between the two sites (Figure 3).

Inverted SWCCs can help confirm heterogeneity or recognize thin units that cannot be sensed by the soil density and elastic moduli alone. If the soil type changes, the water content at the same capillary head will also change (Fredlund and Xing, 1994). Because the seismic velocity is most sensitive to the change in water saturation in near-saturation conditions (Bachrach and Nur, 1998), so may the SWCC inverted from seismic velocity resolve changes in average water saturation at the same capillary head and help determine soil type changes. In the middle seismic layers at both sites, the shift in the SWCC to a lower value indicates the presence of sand units in the layer (Figure 4). If a clay layer contains sand units, the average water saturation will be lower than in a homogeneous clay layer at the same capillary head. A combination of the results of inverted soil density, elastic moduli, and SWCC suggests that the middle layers at both sites may contain sand (Figure 4).

Inverted water saturation, bulk density, and porosity appear consistent with results from laboratory tests from a well near site B (Figure 5). The laboratory water content and bulk density are directly measured on soil cores from the well, and porosity is calculated from these measurements (Lorenzo et al., 2014). Trends in the inverted results at site B match laboratory results throughout the well. Most of the inverted soil property values are within the error range of laboratory results. Because velocity is more sensitive to the change in water saturation than other soil properties, inverted water saturation has the smallest error ($\pm 0.1\%$) compared with errors in other inverted soil properties (which vary from $\pm 1\%$ to $\pm 20\%$) (Figures 3–5). In the inverted and laboratory results, the water saturation shifts to lower values from the first layer to the second layer, and it shifts to higher values from the second to the third layer. As previously mentioned, the shift in water saturation can help to detect seismically unresolvable thin layers. In the first organic clay layer, the inverted and laboratory-based bulk density and porosity show the largest differences. One explanation of these differences is that the inverted soil properties represent average values over the seismic survey area (which covers $\sim$100 m) and may not represent properties at the specific well location. In organic clay, soil properties may have a larger lateral variation because of the difference in organic content.

Comparison of inversion quality between different seismic layers

Within each seismic layer, the corresponding soil behavior types (from CPT data) may vary and so they do not meet the homogeneity assumption of the velocity prediction model. The quality of inversion is best (with a small misfit of 2%) within the deepest layer (Figure 2). The difference between the inverted and geotechnical soil properties are also smallest within the deepest layers (Figure 3). For the top and middle seismic layers, the soil behavior types are a mixture of clay and organic content or sand. Only for the bottom seismic layer is the soil type homogeneous clay. One of the assumptions of the Hertz-Mindlin and Biot-Gassmann theories is that the porous medium is homogeneous (Wang, 2001). Thus, the inversion works best in the relatively homogeneous clay-rich layer in our three-layer seismic model.

Inversion results near the top of the first layer, corresponding to the very near-surface soils (<5 m), unexpectedly predict a velocity that is higher than that seen in the field velocity profile (Figure 2). An interesting possibility is that seismic velocity calculations overestimate the true saturation, which may be lowered by evaporation across the soil surface. In our velocity prediction model, water saturation is determined from the SWCC, which does not account for evaporation effects. As a result, the predicted water saturation from SWCC is greater than in the true field conditions, and the calculated P-wave velocity is larger than the actual field velocity.

There is flexibility with the application of our suggested workflow in future studies. Herein, our attempt at soil property inversion begins with a general velocity prediction model but without any empirical relationship to either simplify the inversion process or reduce possible errors such as those that can arise from using the wrong empirical relationship for a certain field setting. Ideally, the incorporation of other empirical relationships, such as porosity versus coordination number and porosity versus depth, requires a good prior knowledge of the geologic setting, which often is not always the case. The influence of grain-size distribution could also be taken into account because in the inversion results, poor sorting leads to a decrease in porosity and an increase in the coordination number. In this study, we use geologic data from geotechnical and laboratory tests to validate our inversion results. Thus, for the inversion, we only use field velocity profiles without the support of extensive geologic data. In other known geologic settings, empirical relationships could be incorporated into the velocity prediction model to achieve a better inversion result. For example, the unexpected increase of porosity with depth observed using laboratory results (Figure 5) could be incorporated into the future work to improve inversion results. With the suggested workflow in this paper, other more complex velocity prediction models (such as those that include the effect of patchy saturation) could also be used to invert for additional soil-property and water-saturation information.

Although geotechnical borehole tests (± 0.1 cm in our case) may have higher vertical resolution than seismic-derived inverted results (>1 m), seismic surveys advantageously provide continuous lateral seismic soil property values that may complement geotechnical borehole tests for lower cost. Between geotechnical test sites, the inverted soil property results can highlight anomalies in the lateral changes of density, elasticity, and water saturation (Figures 3 and 4). Based on the magnitude and the location of these anomalies, additional geotechnical tests can be proposed and sited efficiently. Another advantage is that soil property inversion uses seismic data, which sample in situ lateral variations of pressure, saturation, and organic content, if any are present. The inversion results can reflect these lateral variations in soil properties between geotechnical boreholes. Currently, seismic soil property inversion for water saturation is most sensitive if it is applied in near fully saturated conditions in which the field P-wave velocity can increase by more than one order of magnitude with only a 1% change in the saturation, and it is also most likely to detect lithologic changes. Inverted soil stratigraphy of this type can improve with the improved resolution of seismic velocity field profiles.

CONCLUSIONS

In shallow (<25 m) near-saturated soil (saturation >99%), we invert for seismic soil properties by minimizing the misfit between field-based velocity profiles and predicted velocity profiles based on the Hertz-Mindlin and Biot-Gassmann theories. CMA-ES optimizes the inversion results by searching for optimal input soil property values that can best explain field velocity profiles.

The inverted density and elastic moduli can be used to interpret major soil types and can detect variations in sand thickness between two field sites. By comparing inversion results with geotechnical results, the inverted soil properties appear valid in general except for one layer, which probably contains seismically unresolvable sandy units.

The inverted SWCC can help recognize thin sand units that are below the original seismic resolution of the field data. Laboratory results validate the inversion results, as well as indicate that the results can be improved with a good prior empirical relationship between porosity and depth. The SWCC shifts to a lower value when the thin unresolvable layers are sandier than the clay-dominated soil. In combination, the inverted density, elastic moduli, and SWCC correspond to soil types that are in agreement with soil types derived from geotechnical data (CPT).

For our three-layer seismic model at our two field sites, the inversion works best in the relatively homogeneous clay-rich bottom layer. Soil within this layer meets the assumption of homogeneity in the Hertz-Mindlin and Biot-Gassmann theories.

Seismic surveys can provide continuous lateral seismic soil property values that may complement geotechnical borehole tests at lower cost. Inversion results can highlight anomalies in lateral changes of density, elasticity, and water saturation to suggest additional geotechnical tests.

Although we use a general velocity model without any empirical relationship in the current workflow, there is flexibility to apply our suggested workflow in future studies. With a known geologic setting, empirical relationships could be incorporated to improve the inversion results. Other velocity prediction models could also be used for the inversion of additional information on soils.

ACKNOWLEDGMENTS

This work is supported by a Shell Exploration and Production Company Grant (2011–2015). We thank H. Pham who helped us with CMA-ES and C. Wilson for valuable discussions. We thank the following for their support with scholarships and graduate assistantship to the first author: Geometrics, Inc., a student travel grant for the Symposium on the Application of Geophysics to Engineering and Environmental Problems; the Donald Towse Memorial Fund awarded by an AAPG Grant-in-Aid; and the EnCana Scholarship and Imagine Resources Scholarship awarded by the Louisiana State University (LSU) Department of Geology and Geophysics. Special thanks go to the LSU Department of Geology and Geophysics for their active support of graduate student research.

APPENDIX A

VELOCITY PREDICTION MODEL

The seismic P-wave velocity (V_P) and S-wave velocity (V_S) are calculated from the effective elastic moduli and bulk density (Dvorkin and Nur, 1996):

$$V_P = \sqrt{\frac{K_{\text{eff}} + \frac{4}{3}G_{\text{eff}}}{\rho_{\text{eff}}}}, \tag{A-1}$$

$$V_S = \sqrt{\frac{G_{\text{eff}}}{\rho_{\text{eff}}}}, \tag{A-2}$$

where K_{eff} is the effective bulk modulus, G_{eff} is the effective shear modulus, and ρ_{eff} is the effective density of the soil matrix with pore fluids and expressed as (Dvorkin and Nur, 1996)

$$\rho_{\text{eff}} = \phi(S_w\rho_w + (1 - S_w)\rho_a) + (1 - \phi)\rho_0, \tag{A-3}$$

where ϕ is the porosity, S_W is the water saturation, ρ_w is the density of water, ρ_a is the density of air, and ρ_0 is the density of the soil grains.

The effective elastic moduli are calculated by the Gassmann fluid substitution theory (Dvorkin and Nur, 1996):

$$K_{\text{eff}} = \frac{K_0\left(\frac{K_m}{K_0 - K_m} + \frac{K_{fl}}{\phi(K_0 - K_{fl})}\right)}{1 + \frac{K_m}{K_0 - K_m} + \frac{K_{fl}}{\phi(K_0 - K_{fl})}}, \tag{A-4}$$

$$G_{\text{eff}} = G_m, \tag{A-5}$$

where K_0 is the bulk modulus of the soil grains, K_m is the bulk modulus of the dry soil matrix, G_m is the shear modulus of the dry soil matrix, and K_{fl} is the bulk modulus of the pore fluids.

We assume the pore fluid to be water and air, so that the bulk modulus of the pore fluids is (Dvorkin and Nur, 1996)

$$K_{fl} = \left(\frac{S_w}{K_w} + \frac{1 - S_w}{K_a}\right)^{-1}, \tag{A-6}$$

where K_w is the bulk modulus of water and K_a is the bulk modulus of air.

Matrix elastic moduli are estimated using the Hertz-Mindlin contact theory (Dvorkin and Nur, 1996):

$$K_m = \sqrt[3]{\frac{C^2(1 - \phi)^2G_0^2}{18\pi^2(1 - \nu)^2}P_{\text{eff}}}, \tag{A-7}$$

$$G_m = \frac{5 - 4\nu}{5(2 - \nu)}\sqrt[3]{\frac{3C^2(1 - \phi)^2G_0^2}{2\pi^2(1 - \nu)^2}P_{\text{eff}}}, \tag{A-8}$$

where C is the coordination number, G_0 is the shear modulus of soil grains, ν is the Poisson's ratio of the soil grains, and P_{eff} is the effective stress.

The SWCC fitting function determines the relationship between the effective water saturation S_e and the capillary head h (Van Genuchten, 1980):

$$S_e = \left[\frac{1}{1 + [ah]^n}\right]^m, \tag{A-9}$$

where a, n, and m are fitting parameters.

Water saturation is related to effective water saturation as (Van Genuchten, 1980)

$$S_w = \frac{S_e(\phi - \theta_r) + \theta_r}{\phi}, \tag{A-10}$$

where θ_r is the residual volumetric water content.

REFERENCES

Allen, J. R. L., 1985, Principles of physical sedimentology: Allen and Unwin.

Avseth, P., J. Dvorkin, G. Mavko, and J. Rykkje, 1998, Diagnosing high-porosity sands for reservoir characterization using sonic and seismic: 68th Annual International Meeting, SEG, Expanded Abstracts, 1024–1027.

Avseth, P., T. Mukerji, and G. Mavko, 2005, Quantitative seismic interpretation: Applying rock physics tools to reduce interpretation risk: Cambridge University Press.

Bachrach, R., and P. Avseth, 2008, Rock physics modeling of unconsolidated sands: Accounting for nonuniform contacts and heterogeneous stress fields in the effective media approximation with applications to hydrocarbon exploration: Geophysics, **73**, no. 6, E197–E209, doi: 10.1190/1.2985821.

Bachrach, R., J. Dvorkin, and A. Nur, 1998, High-resolution shallow-seismic experiments in sand, Part II: Velocities in shallow unconsolidated sand: Geophysics, **63**, 1234–1240, doi: 10.1190/1.1444424.

Bachrach, R., J. Dvorkin, and A. M. Nur, 2000, Seismic velocities and Poisson's ratio of shallow unconsolidated sands: Geophysics, **65**, 559–564, doi: 10.1190/1.1444751.

Bachrach, R., and A. Nur, 1998, High-resolution shallow-seismic experiments in sand, Part I: Water table, fluid flow, and saturation: Geophysics, **63**, 1225–1233, doi: 10.1190/1.1444423.

Bayer, P., E. Duran, R. Baumann, and M. Finkel, 2009, Optimized groundwater drawdown in a subsiding urban mining area: Journal of Hydrology, **365**, 95–104, doi: 10.1016/j.jhydrol.2008.11.028.

Bayer, P., and M. Finkel, 2007, Optimization of concentration control by evolution strategies: Formulation, application, and assessment of remedial solutions: Water Resources Research, **43**, W02410, doi: 10.1029/2005WR004753.

Bell, F. G., 1992, Engineering properties of soils and rocks: Butterworth-Heinemann Ltd.

Biot, M. A., 1962, Mechanics of deformation and acoustic propagation in porous media: Journal of Applied Physics, **33**, 1482–1498, doi: 10.1063/1.1728759.

Bishop, A. W., I. Alpan, G. E. Blight, and I. B. Donald, 1960, Factors controlling the strength of partly saturated cohesive soils: Presented at the Research Conference on Shear Strength of Cohesive Soils.

Crane, J. M., 2013, Effects of stress and water saturation on seismic velocity and attenuation in near surface sediments: Ph.D. dissertation, Louisiana State University.

Digby, P. J., 1981, The effective elastic moduli of porous granular rocks: Journal of Applied Mechanics, **48**, 803–808, doi: 10.1115/1.3157738.

Dutta, T., G. Mavko, and T. Mukerji, 2010, Improved granular medium model for unconsolidated sands using coordination number, porosity, and pressure relations: Geophysics, **75**, no. 2, E91–E99, doi: 10.1190/1.3333539.

Dvorkin, J., and A. Nur, 1996, Elasticity of high-porosity sandstones: Theory for two North Sea data sets: Geophysics, **61**, 1363–1370, doi: 10.1190/1.1444059.

Fredlund, D. G., 1991, How negative can pore-water pressures get?: Geotechnical News, **9**, 44–46.

Fredlund, D. G., 1995, The scope of unsaturated soil mechanics: An overview, *in* E. E. Alonso , and P. Delage, eds., Proceedings of the First International Conference on Unsaturated Soils, vol. 3: Balkema, 1155–1177.

Fredlund, D. G., and H. Rahardjo, 1993a, An overview of unsaturated soil behaviour: *in* S. L. Houston, and W. K. Wray, eds., Proceedings of sessions of ASCE Convention: American Society of Civil Engineers, Specialty Series on Unsaturated Soil Properties, 1–31.

Fredlund, D. G., and H. Rahardjo, 1993b, Soil mechanics for unsaturated soils: John Wiley & Sons.

Fredlund, D. G., and A. Xing, 1994, Equations for the soil-water characteristic curve: Canadian Geotechnical Journal, **31**, 521–532, doi: 10.1139/t94-061.

Fredlund, D. G., A. Xing, M. D. Fredlund, and S. L. Barbour, 1996, The relationship of the unsaturated soil shear to the soil-water characteristic curve: Canadian Geotechnical Journal, **33**, 440–448, doi: 10.1139/t96-065.

Gassmann, F., 1951, Elastic waves through a packing of spheres: Geophysics, **16**, 673–685, doi: 10.1190/1.1437718.

Gilman, K., 1994, Hydrology and wetland conservation: John Wiley & Sons.

Grelle, G., and F. M. Guadagno, 2009, Seismic refraction methodology for groundwater level determination: "Water seismic index": Journal of Applied Geophysics, **68**, 301–320, doi: 10.1016/j.jappgeo.2009.02.001.

Hansen, N., 2006, The CMA evolution strategy: A comparing review, *in* P. Larrañaga, J. A. Lozano, I. Inza, and E. Bengoetxea, eds., Towards a new evolutionary computation: Springer, 75–102.

Hansen, N., 2011, The CMA evolution strategy: A tutorial, http://www.lri.fr/~hansen/cmatutorial.pdf, accessed 6 February 2015.

Harris, J. B., 2009, Hammer-impact SH-wave seismic reflection methods in neotectonic investigations: General observations and case histories from the Mississippi Embayment, USA: Journal of Earth Science, **20**, 513–525, doi: 10.1007/s12583-009-0043-y.

Hayashi, K., T. Inazaki, K. Kitao, and T. Kita, 2013, Statistical soil type estimation using cross-plots of S-wave velocity and resistivity in Japanese levees: Presented at Symposium on the Application of Geophysics to Engineering and Environmental Problems.

Hertz, H., 1882, On the contact of rigid elastic solids and on hardness, *in* D. E. Jones, and G. A. Schott, eds., Miscellaneous papers by H. Hertz: MacMillan, 163–183.

Ikelle, L. T., and L. Amundsen, 2005, Introduction to petroleum seismology: SEG.

Johnson, D. L., 2001, Theory of frequency dependent acoustics in patchy-saturated porous media: Journal of the Acoustical Society of America, **110**, 682–694, doi: 10.1121/1.1381021.

Leong, E. C., and H. Rahardjo, 1997, Review of soil-water characteristic curve equations: Journal of Geotechnical and Geoenvironmental Engineering, **123**, 1106–1117, doi: 10.1061/(ASCE)1090-0241(1997)123:12(1106).

Lorenzo, J. M., J. Hicks, and E. E. Vera, 2014, Integrated seismic and cone penetration test observations at a distressed earthen levee: Marrero, Louisiana, USA: Engineering Geology, **168**, 59–68, doi: 10.1016/j.enggeo.2013.10.019.

Lu, N., and W. J. Likos, 2006, Suction stress characteristic curve for unsaturated soil: Journal of Geotechnical and Geoenvironmental Engineering, **132**, 131–142, doi: 10.1061/(ASCE)1090-0241(2006)132:2(131).

Lu, Z., and J. M. Sabatier, 2009, Effects of soil water potential and moisture content on sound speed: Soil Science Society of America Journal, **73**, 1614–1625, doi: 10.2136/sssaj2008.0073.

Masoni, I., W. Zhou, R. Brossier, L. Métivier, S. Operto, and J. Virieux, 2014, Near-surface full waveform inversion using surface waves and reflected waves: 76th Annual International Conference and Exhibition, EAGE, Extended Abstracts, doi: 10.3997/2214-4609.20140531.

Mavko, G., T. Mukerji, and J. Dvorkin, 2009, The rock physics handbook: Tools for seismic analysis of porous media: Cambridge University Press.

Mezura-Montes, E., and C. A. Coello Coello, 2011, Constraint-handling in nature-inspired numerical optimization: Past, present and future: Swarm and Evolutionary Computation, **1**, 173–194, doi: 10.1016/j.swevo.2011.10.001.

Mindlin, R. D., 1949, Compliance of elastic bodies in contact: Journal of Applied Mechanics, **16**, 259–268.

Mittal, B., H. Yi, V. M. Puri, A. S. McNitt, and C. F. Mancino, 2004, Bulk mechanical behavior of rootzone sand mixtures as influenced by particle shape, moisture and peat: Particle and Particle Systems Characterization, **21**, 303–309, doi: 10.1002/ppsc.200400934.

Murphy, W. F., 1982, Effects of microstructure and pore fluids on the acoustic properties of granular sedimentary materials: Ph.D. dissertation, Stanford University.

Nimmo, J. R., 2004, Porosity and pore size distribution: *in* D. Hillel, ed., Encyclopedia of Soils in the Environment, vol. 3: Elsevier, 295–303.

Revil, A., and H. Mahardika, 2013, Coupled hydromechanical and electromagnetic disturbances in unsaturated porous materials: Water Resources Research, **49**, 744–766, doi: 10.1002/wrcr.20092.

Robertson, P. K., 1990, Soil classification using the cone penetration test: Canadian Geotechnical Journal, **27**, 151–158, doi: 10.1139/t90-014.

Takahashi, T., and S. Tanaka, 2009, Rock physics model for interpreting elastic properties of soft sedimentary rocks: International Journal of the Japanese Committee for Rock Mechanics, **4**, 53–59.

Terzaghi, K., 1996, Soil mechanics in engineering practice: John Wiley & Sons.

Van Genuchten, M. T., 1980, A closed-form equation for predicting the hydraulic conductivity of unsaturated soils: Soil Science Society of America Journal, **44**, 892–898, doi: 10.2136/sssaj1980.03615995004400050002x.

Velea, D., F. D. Shields, and J. M. Sabatier, 2000, Elastic wave velocities in partially saturated Ottawa sand: Soil Science Society of America Journal, **64**, 1226–1234, doi: 10.2136/sssaj2000.6441226x.

Walmsley, M. E., 1977, Physical and chemical properties of peat: Muskeg and the Northern Environment in Canada: University of Toronto Press, 83–129.

Waltham, T., 2001, Foundations of engineering geology: CRC Press.

Walton, K., 1987, The effective elastic moduli of a random packing of spheres: Journal of the Mechanics and Physics of Solids, **35**, 213–226, doi: 10.1016/0022-5096(87)90036-6.

Wang, Z., 2001, Fundamentals of seismic rock physics: Geophysics, **66**, 398–412, doi: 10.1190/1.1444931.

Zimmer, M. A., M. Prasad, G. Mavko, and A. Nur, 2007, Seismic velocities of unconsolidated sands: Part 1 — Pressure trends from 0.1 to 20 MPa: Geophysics, **72**, no. 1, E1–E13, doi: 10.1190/1.2399459.